Journal of Alloys and Compounds 509 (2011) 7738–7741

Contents lists available at ScienceDirect

Journal of Alloys and Compounds

journal homepage: www.elsevier.com/locate/jallcom

Study on magnetic and dielectric properties of $YMnO_3$ ceramics

Chao Zhang[a,b], Jie Su[a], Xiaofei Wang[a,b], Fengzhen Huang[a], Junting Zhang[a], Yaoyang Liu[a], Liang Zhang[a], Kangli Min[a], Zhijun Wang[a], Xiaomei Lu[a,*], Feng Yan[c,*], Jinsong Zhu[a]

[a] National Laboratory of Solid State Microstructures, Nanjing University, Nanjing 210093, China
[b] School of Physics and Engineering, Henan University of Science and Technology, Luoyang 471003, China
[c] Department of Applied Physics, Hong Kong Polytechnic University, Hong Kong, China

ARTICLE INFO

Article history:
Received 14 January 2011
Received in revised form 22 April 2011
Accepted 26 April 2011
Available online 5 May 2011

Keywords:
Magnetic and dielectric properties
$YMnO_3$ ceramics

ABSTRACT

The magnetic and dielectric properties were investigated in the hexagonal $YMnO_3$ ceramics synthesized by sol–gel method. An antiferromagnetic order about 70 K and a weak ferromagnetic order at 5 K have been detected in $YMnO_3$ ceramics. In addition, we observed also the exchange-bias (EB) effect at low temperatures and it may originate from exchange coupling at the interface between ferromagnetic and antiferromagnetic orders for the co-existence of these two orders in some temperature region in hexagonal $YMnO_3$. Furthermore, the dielectric measurements showed two thermally activated relaxation behaviors following the Arrhenius law in 290–430 K and above 500 K in $YMnO_3$ ceramics and they can be explained as the dipolar effects associated with the charge carrier hopping between Mn^{2+} and Mn^{3+} and oxygen vacancy, respectively.

1. Introduction

Recently, the multiferroics have been extensively studied in several manganese oxides such as perovskite $RMnO_3$, hexagonal $RMnO_3$, and RMn_2O_5 [1–5]. The yttrium and rare-earth manganite $RMnO_3$ form an interesting family showing a wide variety of physical properties. Hexagonal $YMnO_3$ (YMO) has the antiferromagnetic (AFM) and the ferroelectric (FE) orders and the transition temperatures of FE and AFM are 900 K (T_c) and ~70 K (T_N), respectively. Electrical polarization in YMO is along the hexagonal *c* axis [6] whereas the magnetic moments of Mn^{3+} lie in the perpendicular plane, forming a triangular, geometrically frustrated network of AFM coupled spins [7,8]. In addition, magneto-capacitive effect has been reported in several manganates and other oxides at low temperature [1,9,10]. In the past several years, the study on the dielectric properties of the YMO thin film, the doped manganate ($Y_{1-x}R_xMnO_3$) films and single crystal has been performed in the temperature range of $T < 100$ K [11,12]. However, the experimental work on the dielectric behavior of YMO ceramics is still scarce. In this paper, the antiferromagnetic, weak ferromagnetic and the exchange bias (EB) effect in hexagonal $YMnO_3$ ceramics at low temperatures are reported and the origin of the EB effect is discussed. Besides, the dielectric properties of YMO ceramics between 290 K and 630 K were studied and the experimental results revealed a peculiar dielectric behavior in YMO ceramics which was different from the one reported by others. They were closely linked with the dipolar effects associated with the charge carrier hopping between Mn^{2+} and Mn^{3+} and oxygen vacancy respectively. Both the magnetic and the dielectric behaviors reported here are useful in understanding the multiferroic property of YMO.

2. Experimental

Synthesis of the $YMnO_3$ ceramics was carried out by a citrate sol–gel route. Stoichiometric amounts of aqueous metal nitrates were prepared by dissolving $Mn(CH_3COO)_2{\cdot}4H_2O$ (99.5%) and $Y(NO_3)_3{\cdot}6H_2O$ (99.99%) powders in a minimum amount of concentrated nitric acid. The total metal ion concentration was kept at around 0.2 M by adding distilled water. The resulting solution was held for 4 h under constant stirring, the molar ratio of total metal ion to citric acid was kept at a ratio of 1:2, an appropriate amount of citric acid was added to this solution under constant stirring. The precursor powder (greyish brown) was then ground and heated at 300 °C for 3 h in air, all of the powders calcined at 900 °C for 10 h in air which enabled the formation of the desired oxides. The resulting powder was ground and pressed into disks of 2 cm diameter and 1 mm thickness under a pressure of 40 MPa. Then the disks were sintered in air at 1100 °C for 15 h and the Pt dot electrodes were sputtered for electrical measurements.

The microstructure of the ceramics was performed by the X-ray powder diffraction (XRD, D/Max-RB) with Cu-Kα radiation and X-ray photoelectron spectroscopy (XPS Thermo ESCALAB 250). The temperature dependence of the magnetization was measured with the zero-field-cooled state (ZFC) and the field-cooled state (FC) with 1000 Oe by a superconducting quantum interference device (SQUID). The dielectric characteristics were evaluated using HP4194A impedance in the frequency range from 100 Hz to 1 MHz and in the temperature from 290 to 630 K.

3. Results and discussion

The X-ray diffraction (XRD) pattern of YMO ceramics is shown in Fig. 1. The diffraction peaks can be indexed on the basis of a hexag-

* Corresponding authors.
E-mail addresses: xiaomeil@nju.edu.cn (X. Lu), apafyan@polyu.edu.cn (F. Yan).

0925-8388/$ – see front matter © 2011 Elsevier B.V. All rights reserved.
doi:10.1016/j.jallcom.2011.04.128

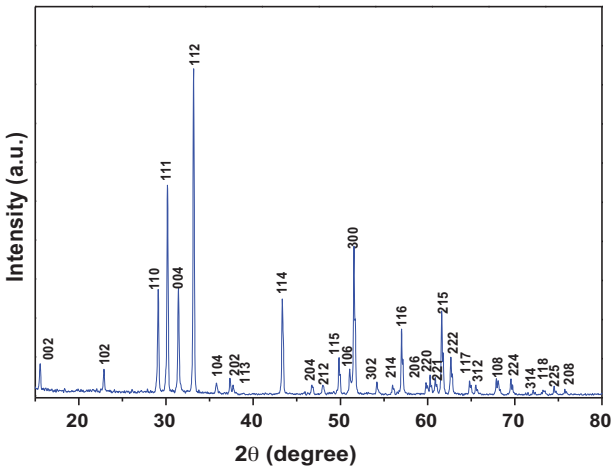

Fig. 1. XRD patterns of YMO ceramics.

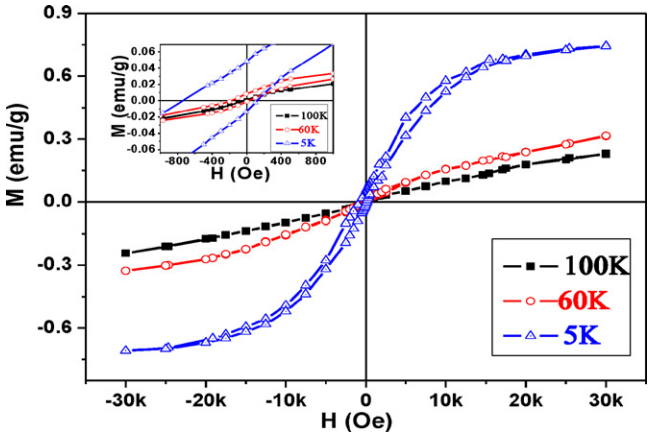

Fig. 3. Typical magnetic-field dependence of the magnetization $M(H)$ at different temperatures for YMO. Inset shows the enlarged view in the low field region.

onal unit cell of space group $P6_3cm$ [7,13,14] and no additional impurity or intermediate phases were observed.

Fig. 2a shows the magnetization as a function of temperature in zero field cooling (ZFC) and field cooling (FC) conditions with 1000 Oe for the YMO ceramics. The magnetization presented a splitting at $T \sim 70$ K and the $d\chi/dT$ showed clearly an anomaly near the antiferromagnetic $T_N \sim 70$ K (Fig. 2b). According to the Curie–Weiss law, the T dependence of the $1/\chi$ above 100 K (paramagnetic state) in the FC was fitted with a negative extrapolated temperature $\theta_{CW} \sim -280$ K (inset of Fig. 2a), higher than previous report [7], implying that the dominant magnetic interaction is AFM. Both the FC and the ZFC curves showed an abrupt increase in magnetization at low temperature. It shows the suppressed AFM and an appearance of the weak ferromagnetism in the bulk manganate.

Fig. 3 shows the dependence of the magnetization M (H) on the magnetic field between ±30 kOe at temperatures of 5 K, 60 K, and 100 K in YMO ceramics, respectively. The M vs H curve at 100 K presented a paramagnetic and a very small hysteresis loop or an antiferromagnetism at 60 K in YMO. But a clear hysteresis displayed at about 5 K on the M vs H curve, shown in the inset of Fig. 3, i.e. a weak ferromagnetism was observed. Thus, the coexistence of the AFM order and the FM order is possible in some temperature range. From the inset of Fig. 3, the hysteresis loop showed a shift toward negative magnetic field and an enhanced coercive field in lower temperature. The appearance of horizontal shift of the hysteresis loop in the sample is called as the exchange bias (EB) effect. Similar phenomena have also been reported in the literature, Borisov et al. [15] and Laukhin et al. [16] reported the electric-field control of exchange bias (EB) effect and Salazar-Alvarez [17] have shown that EB effect can also be observed in the nano-particles with core–shell structure, composed of an AFM core and a FM shell. The appearance of horizontal shift of the hysteresis loop in our sample may originate from the exchange coupling at the interface of FM and AFM orders. To evaluate the magnitude of the exchange bias (EB), H_{EB} was defined as $H_{EB} = -(H_1 + H_2)/2$ and the H_1 and H_2 are the left and right coercive fields. The value of H_{EB} was about 310 and 66 Oe at 5 K and 60 K, respectively, i.e. the H_{EB} increased with the decreasing temperature for the ferromagnetism will enhance with decreasing temperature and more uncompensated spins are aligned and rotated. These spins will cause a change in the magnetic configuration at the interface of the AFM/FM, more and more frozen-in spins are created and the exchange interaction is enhanced. Thus, the H_{EB} increased at lower temperature. Actually, the shifted loop indicates that a fraction of the uncompensated moments was pinned after field cooling process for a very local anisotropy and cannot reverse [18–22].

Fig. 4 shows the temperature dependence of dielectric constant ε and dielectric loss tan δ, respectively. Three peaks appeared in the curves of tan δ and ε as a function of temperature in different measuring frequencies, except the one at low temperature ($T < 350$ K) cannot be discerned clearly in ε. The relaxation behavior can be observed in the YMO ceramic in 290–430 K and above 500 K in tan δ, they can be referred to as the low-temperature dielectric relaxation (LTDR) and high-temperature dielectric relaxation (HTDR), respectively. Both the LTDR and HTDR have frequency dispersion, the

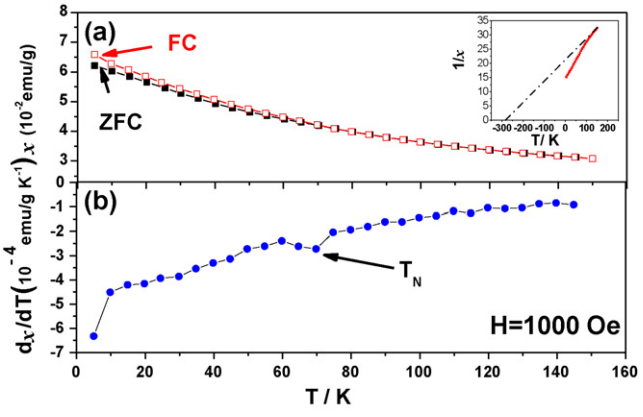

Fig. 2. (a) T dependence of the magnetization curves of YMO in ZFC and FC at 1000 Oe. Inset shows reciprocal susceptibility $1/\chi$ vs T in FC; (b) T dependence of the derivative of the dc magnetic susceptibility ($d\chi/dT$) at 1000 Oe.

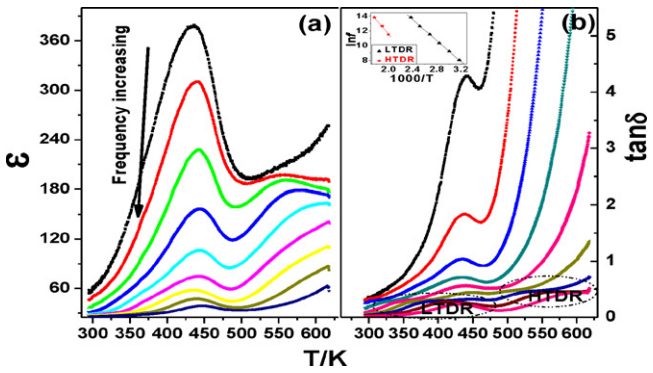

Fig. 4. T dependence of ε, tan δ on the frequencies (10^2,$10^{2.5}$, 10^3, $10^{3.5}$, 10^4, $10^{4.5}$, 10^5, $10^{5.5}$, and 10^6 Hz). Inset (b) gives the Arrhenius plot for the relaxation peak for LTDR and HTDR.

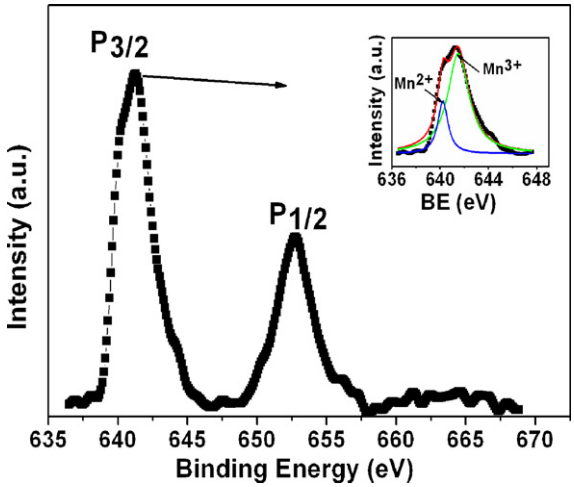

Fig. 5. XPS spectra of Mn 2p lines for the binding energy between 635 and 670 eV. Inset shows the Lorentzian fitting of the Mn 2p3/2 core level for YMO ceramics.

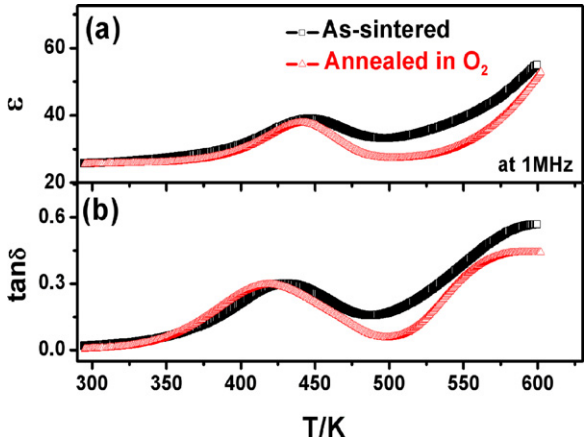

Fig. 6. Effects of O_2 annealing on (a) dielectric constant ε and (b) tan δ in YMO ceramics at 1 MHz.

temperature of the dissipation peak shifted to a higher temperature range with increasing frequency and they are a thermally excited relaxation process. Generally, for a thermally activated relaxation process, by using an Arrhenius expression:

$$f_m = f_0 \exp\left(\frac{-E}{k_B T_p}\right)$$

where f_m, f_0, E, k_B, T_p are the peak frequency, the characteristic frequency at infinite temperature, the activation energy, the Boltzmann constant and the peak temperature, respectively. The activation energy E follows Arrhenius law as shown in inset of Fig. 4b are 0.61 eV and 0.89 eV for the LTDR and HTDR, respectively.

To clarify the mechanism of dielectric relaxation in YMO, the valence variation of Mn ions was analyzed by XPS measurements at room temperature. Fig. 5 shows the XPS spectra of Mn 2p regions of YMO ceramics and the Lorentzian fitting curves are also shown in the inset of Fig. 5. The $2p_{3/2}$ peak for Mn could be split into two peaks in relation to Mn^{2+} and Mn^{3+} and the binding energy for Mn^{2+} $2p_{3/2}$ and Mn^{3+} $2p_{3/2}$ are 640.22 and 641.46 eV, respectively, the intensity ratio of the Mn^{2+}/Mn^{3+} component is about 1/4 for the sample. The most likely origin of Mn^{2+} ions in the YMO ceramics was the presence of oxygen vacancies introduced in the fabrication process of sample. Then the ordering of Mn^{2+}/Mn^{3+} can produce the polar clusters and the thermally activated dielectric relaxation process comes into being [23]. The LTDR may be related to two-site polaron hopping process of charge transfer between Mn^{2+} and Mn^{3+}. For the relaxation in high temperature (HTDR), the activation energy (0.89 eV) is very close to the activation energy for the motion of oxygen vacancy. In the cases of $Ba(Fe_{1/2}Nd_{1/2})O_3$ and $Bi_{4-x}La_xTi_3O_{12}$ ceramics [24,25], the dielectric relaxation can also be observed with the activation energies about 0.83–1.0 eV. They referred the relaxation to a defect ordering in $Ba(Fe_{1/2}Nd_{1/2})O_3$ and $Bi_{4-x}La_xTi_3O_{12}$, respectively, these results seem to be similar to those of our case for the HTDR. Fig. 6 presents the comparison of the dielectric behaviors for the as-sintered and the O_2-annealed YMO samples. The relaxation peak of low temperature was just slightly effected by O_2-annealing (the relaxation temperature slightly shifted toward lower temperature), and there was almost no change in the height of dielectric peak. On the other hand, the high temperature relaxation peak of ε and corresponding dielectric loss tan δ peak were significantly suppressed by O_2-annealing. It indicates that the HTDR was an extrinsic mechanism and should be related with the oxygen vacancy. These results confirm that the LTDR is the intrinsic one which originates from the carries hopping process between Mn^{2+} and Mn^{3+} and the HTDR is due to the oxygen vacancy. At the same time we note that there is an approximately ten-fold drop of the dielectric peak height ε and tan δ about 430 K with the increase of measuring frequency (shown in Fig. 4) and the peak positions in dielectric constant (ε) were no change almost, only slightly shifted to lower temperatures with the increase of the measuring frequency. It may be related to some kind of phase transition and further investigation is needed for the details.

4. Conclusion

Hexagonal YMO ceramics were synthesized by sol–gel method and magnetic properties of $YMnO_3$ were investigated using dc magnetizations. Anti-ferromagnetic order appeared about 70 K and the weak ferromagnetic properties were detected at 5 K. The exchange-bias effect in hexagonal YMO at low temperatures was also observed and it is attributed to an exchange coupling at the interface between an antiferromagnetic and a ferromagnetic order in the YMO. Two dielectric relaxation behaviors appeared about 290–430 K and above 510 K, respectively, they are the thermally activated process following the Arrhenius law.

The dipolar effects associated with the charge carrier hopping between Mn^{2+} and Mn^{3+} and the relaxation of oxygen vacancy were used to explain the results. Besides, the anomaly of dielectric constant and the loss (tan δ) about 430 K may be related to some kind of phase transition.

Acknowledgments

This work was supported by the National Science Foundation of China (Grant Nos. 50832002, 51002075 and 50972056), the 973 Project of MOST (Grant No. 2009CB929501), and NCET-06-0443.

References

[1] T. Kimura, T. Goto, T. Arima, Y. Tokura, Nature (Lond.) 426 (2003) 55.
[2] C.Y. Yen, S.R. Jian, Y.S. Lai., J.Y. Juang, J. Alloys Compd. 508. (2010) 523–527.
[3] Y.J. Wu, L.H. Tang, H.L. Li, X.M. Chen, J. Alloys Compd. 496 (2010) 269–272.
[4] B. Lorenz, A.P. Litvinchuk, C.W. Chu, Phys. Rev. Lett. 92 (2004) 087204.
[5] N. Hur, S. Park, A. Sharma, J.S. Ahn, S. Guha, Nature (London) 429 (2004) 392–395.
[6] B.B. Van Aken, T.T.M. Palstra, N. Spaldin, Nat. Mater. 3 (2004) 164–170.
[7] A. Muñoz, J.A. Alonso, M.J. Martínez-Lope, Phys. Rev. B 62 (2000) 9498–9510.
[8] M. Fiebig, D. Frölich, R.V. Pisarev, Phys. Rev. Lett. 84 (2000) 5620–5623.
[9] F. Schrettle, P. Lunkenheimer, J. Hemberger, V.Yu. Ivanov, A.A. Mukhin, A.M. Balbashov, A. Loidl, Phys. Rev. Lett. 102 (2009) 207208.
[10] T. Goto, T. Kimura, G. Lawes, A.P. Ramirez, Y. Tokura, Phys. Rev. Lett. 92 (2004) 257201.

[11] I. Fina, X. Martí, L. Fàbrega, F. Sànchez, J. Fontcuberta, Thin Solid Films 518 (2010) 4710–4713.
[12] J.A. Moreira, A. Almeida, W.S. Ferreira, S.M.F. Vilela, P.B. Tavares, B. Kundys, W. Prellier, J. Appl. Phys. 107 (2010) 024108.
[13] Y. Ma, X.M. Chen, Y.J. Wu, Ceram. Int. 36 (2010) 727–731.
[14] H. Fukumura, S. Matsui, H. Harima, K. Kisoda, N. Fujimura, J. Phys. Condens. Matter 19 (2007) 365239.
[15] P. Borisov, et al., Phys. Rev. Lett. 94 (2005) 117203.
[16] V. Laukhin, V. Skumryev, D. Hrabovsky, C. Ferrater, J.F. Bobo, J. Fontcuberta, Phys. Rev. Lett. 97 (2006) 227201.
[17] G. Salazar-Alvarez, J. Sort, S. Suriñach, M. Dolors Baró, J. Nogués, J. Am. Chem. Soc. 129 (2007) 9102–9108.
[18] M. Ali, P. Adie, C.H. Marrows, D. Greig, B.J. Hickey, R.L. Stamps, Nat. Mater. 6 (2007) 70–75.
[19] S. Vijayanand, M.B. Mahajan, H.S. Potdar, P.A. Joy, Phys. Rev. B 80 (2009) 064423.
[20] A. Querejeta, A. Varela, M. Parras, F. del Monte, M. García-Hernández, J.M. González-Calbet, Chem. Mater. 21 (2009) 1898–1905.
[21] J. Dho, M.G. Blamire, Appl. Phys. Lett. 87 (2005) 252504.
[22] A. Tomou, D. Gournis, I. Panagiotopoulos, Y. Huang, G.C. Hadjipanayis, B.J. Kooi, J. Appl. Phys. 99 (2006) 123915.
[23] Xiaobo Wu, Xiaofei Wang, Yunfei Liu, Wei Cai, Song Peng, Fengzhen Huang, Xiaomei Lu, Feng Yan, Jinsong Zhu, Appl. Phys. Lett. 95 (2009) 182903.
[24] Z. Wang, X.M. Chen, L. Ni, X.Q. Liu, Appl. Phys. Lett. 90 (2007) 192905.
[25] Y.Y. Yao, C.H. Song, P. Bao, D. Su, X.M. Lu, J.S. Zhu, Y.N. Wang, J. Appl. Phys. 95 (2004) 3126–3130.